remote sensing

MDPI

Article

Research on the Algorithm of Lake Surface Height Inversion in Qinghai Lake Based on Sentinel-3A Altimeter

Chuntao Chen [1], Xiaoqing Li [1], Jianhua Zhu [2], Hailong Peng [3,4], Youhua Xue [5], Wanlin Zhai [2], Mingsen Lin [4], Yufei Zhang [3,4], Jiajia Liu [1] and Yili Zhao [6,*]

1 School of Ocean, Yantai University, Yantai 264005, China; chenchuntao@ytu.edu.cn (C.C.); lixiaoqing@s.ytu.edu.cn (X.L.); hyxyjw@ytu.edu.cn (J.L.)
2 National Ocean Technology Center, Ministry of Natural Resources, Tianjin 300112, China; besmile@263.net (J.Z.); zwl13032@163.com (W.Z.)
3 Key Laboratory of Space Ocean Remote Sensing and Application, Ministry of Natural Resources, Beijing 100081, China; phl@mail.nsoas.org.cn (H.P.); zhyf@mail.nsoas.org.cn (Y.Z.)
4 National Satellite Ocean Application Service, Ministry of Natural Resources, Beijing 100081, China; mslin@mail.nsoas.org.cn
5 Hainan Aerospace Technology Innovation Center, Wenchang 571300, China; xueyouhua@hn-atic.com
6 School of Marine Technology and Geomatics, Jiangsu Ocean University, Lianyungang 222005, China
* Correspondence: yili.zhao@jou.edu.cn; Tel.: +86-15022333051

Abstract: Lakes are a crucial component of inland water bodies, and changes in their water levels serve as key indicators of global climate change. Traditional methods of lake water level monitoring rely heavily on hydrological stations, but there are problems such as regional representativeness, data stability, and high maintenance costs. The satellite altimeter is an essential tool in lake research, with the Synthetic Aperture Radar (SAR) altimeter offering a high spatial resolution. This enables precise and quantitative observations of lake water levels on a large scale. In this study, we used Sentinel-3A SAR Radar Altimeter (SRAL) data to establish a more reasonable lake height inversion algorithm for satellite-derived lake heights. Subsequently, using this technology, a systematic analysis study was conducted with Qinghai Lake as the case study area. By employing regional filtering, threshold filtering, and altimeter range filtering techniques, we obtained effective satellite altimeter height measurements of the lake surface height. To enhance the accuracy of the data, we combined these measurements with GPS buoy-based geoid data from Qinghai Lake, normalizing lake surface height data from different periods and locations to a fixed reference point. A dataset based on SAR altimeter data was then constructed to track lake surface height changes in Qinghai Lake. Using data from the Sentinel-3A altimeter's 067 pass over Qinghai Lake, which has spanned 96 cycles since its launch in 2016, we analyzed over seven years of lake surface height variations. The results show that the lake surface height exhibits distinct seasonal patterns, peaking in September and October and reaching its lowest levels in April and May. From 2016 to 2023, Qinghai Lake showed a general upward trend, with an increase of 2.41 m in lake surface height, corresponding to a rate of 30.0 cm per year. Specifically, from 2016 to 2020, the lake surface height rose at a rate of 47.2 cm per year, while from 2020 to 2022, the height remained relatively stable.

Keywords: lake surface height; SAR altimeter; Sentinel-3A; GPS buoy; Qinghai Lake

check for updates

Academic Editor: Pavel Kishcha

Received: 19 December 2024
Revised: 7 February 2025
Accepted: 9 February 2025
Published: 14 February 2025

Citation: Chen, C.; Li, X.; Zhu, J.; Peng, H.; Xue, Y.; Zhai, W.; Lin, M.; Zhang, Y.; Liu, J.; Zhao, Y. Research on the Algorithm of Lake Surface Height Inversion in Qinghai Lake Based on Sentinel-3A Altimeter. *Remote Sens.* **2025**, *17*, 647. https://doi.org/10.3390/rs17040647

Copyright: © 2025 by the authors. Licensee MDPI, Basel, Switzerland. This article is an open access article distributed under the terms and conditions of the Creative Commons Attribution (CC BY) license (https://creativecommons.org/licenses/by/4.0/).

1. Introduction

Although inland water bodies comprise less than one percent of the Earth's total water volume, they are crucial for life on Earth and play a significant role in climate change.

Lakes, as integral components of the hydrosphere, act as bridges linking interactions among the Earth's four major spheres—the atmosphere, lithosphere, biosphere, and hydrosphere. They are closely interconnected with these spheres and serve vital roles in local environmental changes, climate regulation, ecological balance, and biodiversity proliferation. Lakes contribute to economic development by regulating river flows, supporting irrigation, providing water resources, facilitating aquatic species propagation, sustaining industry, enabling shipping, improving regional ecological conditions, and aiding mineral resource development. In these ways, they exert a profound impact on human society [1–3]. Furthermore, lakes are highly sensitive to global climate change, particularly in terms of water resource depletion, environmental degradation, and the increasing frequency of water-related disasters. As a primary source of water for humans, lakes play a central role in many aspects of life and have significant implications across various fields. The evolution of lakes—whether through their formation, expansion, decline, or drying up—reflects the combined influences of local and global tectonic activity and climate change [3].

In the assessment and management of lake water resources, three key variables are typically considered: water level, area, and volume, which are generally positively correlated. The water level of a lake is a crucial indicator, with its long-term fluctuations reflecting regional climate changes. These fluctuations are influenced by both climatic factors and human activities. The stability and sustainability of lake water levels can significantly impact human livelihoods and production [4–6]. Water level variations are driven by a variety of factors, including rainfall, evaporation, water flow, and seepage, as well as the combined effects of seasons, climate, water sources, and human interventions. The accurate monitoring of lake water level changes is essential for understanding regional climate patterns and providing a scientific basis for the sustainable use and protection of water resources. Long-term studies of lake water level fluctuations can reveal broader trends, offering valuable insights for scientific decision making. Traditional methods of lake water level monitoring rely heavily on hydrological stations, which serve as a primary data source for studying water level changes and associated climate impacts [4,5]. In China, hydrological stations are established in larger lakes to monitor water levels and support related research. However, due to the high construction and maintenance costs, it is not feasible to install stations for all lakes. Moreover, for large lakes, a single hydrological station may not adequately capture water level variations across the entire lake, leading to issues of representativeness. Additionally, the reliability of data from these stations can be compromised by problems with the station benchmarks. For instance, the Qinghai–Tibet Plateau, the largest and highest plateau lake region on Earth, experiences approximately two strong earthquakes every decade [6]. Such earthquake events can significantly affect the benchmarks of hydrological stations, thereby undermining the accuracy and reliability of the water level data.

With the development of remote sensing technology, it has become possible to obtain large-scale and long-time series datasets on lake water level changes using remote sensing. Satellite altimeters have obvious advantages over hydrological stations: one is that satellite altimeters make observations from space, so topographic changes such as earthquakes do not influence their data; and second, they have the advantage of being able to make synchronous observations over large areas, which have better lake representativeness. Since the launch of the first satellite-borne active microwave remote sensing spacecraft, Skylab, in 1973, and the operational TOPEX/Poseidon (T/P) altimeter satellite in 1992, altimetry technology has been continuously developed, with its measurement accuracy improving to 2–3 cm [7–10]. The application of satellite radar altimeters has expanded from monitoring oceans to tracking water level changes in lakes, rivers, and other inland waters, thanks to improvements in accuracy. Key applications include lake water level

monitoring [7–19], lake water level and storage volume estimation [19–24], lakes and climate change [4–6,20,22], large river water level monitoring [25–29], and wetland water level changes [22,25,30–33]. Initially, research on inland water bodies relied on data from single altimeter satellites. However, with the successful launch of additional altimeter satellites in the 21st century—such as Jason-1, Jason-2, GFO, ENVISAT, ICESat, CryoSat-2, HY-2A, Jason-3, Sentinel-3, HY-2B, HY-2C, and HY-2D—researchers are now able to use data from two or more radar altimeters [13,16,20,22–25,27,31–36]. This has enabled the generation of longer time series datasets, improving both the temporal span and spatial resolution of inland water body water level measurements. In 2011, the French Laboratory of Space Geophysical and Oceanographic Studies (LEGOS) initiated the HYDROWEB dataset for monitoring large global lakes. Following this, the United States Department of Agriculture established the Global Reservoir and Lake Monitoring (GRLM) system, while the European Space Agency created the "The River and Lake" global river and lake water level monitoring database. Additionally, Germany developed a global inland water body hydrological time series dataset (DAHITI). These global monitoring datasets are all based on satellite altimeter data [36].

Satellite altimeters encounter two primary challenges when measuring lake water levels. First, it is crucial to ensure that the satellite altimeter's footprint is not contaminated by land. However, the pulse footprint of the T/P and Jason series altimeter satellites ranges from 2 to 7 km, and it takes approximately 3 to 5 s to switch from land mode to ocean mode [37]. This transition limits the number of effective measurement points available for calculating lake water levels. Second, the sea surface height inversion algorithms used for ocean measurements are not suitable for lake water level inversion [38,39]. To ensure accurate lake water level measurements with satellite altimeters, it is essential to calibrate the altimeters specifically for lakes and develop methods for lake water level inversion. Using a standardized calibration system to calibrate different altimeter satellites can establish the continuity and consistency of measurements across various altimeters, enabling the creation of long-term time series datasets. This is a necessary foundation for hydrological studies on interannual and decadal changes.

Launched in February 2016, the Sentinel-3A satellite is part of the Copernicus program, a European Earth observation mission initiative designed to monitor the Earth's land, oceans, atmosphere, and ice, as well as to detect emergencies. The mission is jointly operated by the European Space Agency (ESA) and the European Organization for the Exploitation of Meteorological Satellites (EUMETSAT), with the ESA responsible for land observation services and the EUMETSAT handling the processing and distribution of ocean data. Sentinel-3A is the first satellite system to provide global coverage in Synthetic Aperture Radar (SAR) mode and to offer a higher along-track resolution [40–42].

The SRAL (SAR Radar Altimeter) is a key component of the Sentinel-3A satellite, consisting of a central electronic chain that includes a radio frequency unit (RFU) and a digital processing unit (DPU) located inside the satellite, as well as a low-gain antenna mounted on the satellite's external panel. The altimeter operates in two frequency bands: the Ku-band (13.575 GHz and bandwidth 350 MHz) and C-band (5.41 GHz and bandwidth 320 MHz). The Ku-band is primarily used for surface height measurements, while the C-band is mainly employed for ionospheric corrections. The SRAL system includes the measurement, calibration, and support modes. The measurement mode is further divided into two radar modes and two tracking modes. The two radar modes are Synthetic Aperture Radar (SAR) mode, which is commonly used, and Low Resolution Mode (LRM), which serves as a backup [41,42]. Level 2 SRAL data are provided in three file types, with the "standard" data file containing 1 Hz and 20 Hz Ku- and C-band parameters. Sentinel-3A SRAL has 385 global orbits, and the 20 Hz Ku-band land measurement tracks are composed

of data points spaced 320 m apart. Due to SRAL's superior spatiotemporal resolution, the Sentinel-3A satellite offers significant potential for water level monitoring. It can effectively minimize the impact of land on the satellite's footprint and provides a higher volume of valid data for lake observations.

This paper focuses on Qinghai Lake for two main reasons. First, Qinghai Lake is the largest lake in China, providing a substantial amount of reliable altimeter data. Second, multiple altimeter satellites, including HY-2A, HY-2B, Sentinel-3A, and Sentinel-3B, pass over the lake. The study uses Sentinel-3A's SRAL data to perform multi-year observations of lake water level changes. Section 2 outlines the experimental conditions at Qinghai Lake, including comparisons between GPS buoy and tide gauge measurements of water levels and geodetic height measurements of satellite nadir points. It also introduces the data sources, which include the Sentinel-3A altimeter, tide gauge data, and GPS buoy measuring system data, along with the methods used for processing these data. Section 3 presents the results of the data processing, covering the accuracy of GPS buoy measurements, geoid height differences, and normalized lake surface heights. Section 4 discusses and analyzes the findings of this study. The Section 5 offers our conclusions based on the results.

2. Materials and Methods

2.1. Experimental Introduction

This paper investigates satellite altimeter observations of lake water levels, specifically considering the impact of land on the footprint of the satellite altimeter's nadir track. To maximize the amount of effective satellite altimeter data, Qinghai Lake was selected for in situ measurement experiments. As the largest lake in China, Qinghai Lake is located in the northeastern part of the Qinghai–Tibet Plateau and plays a crucial role in maintaining the ecological security of the region. As shown in Figure 1, the lake stretches 106 km in length and 63 km in width, with geographic coordinates ranging from 99°36′E to 100°50′E and 36°32′N to 37°15′N. The terrain is higher in the northwest and lower in the southeast, with an average water depth of 21 m, a maximum depth of 32.8 m, and a lake surface elevation of 3196 m [43,44].

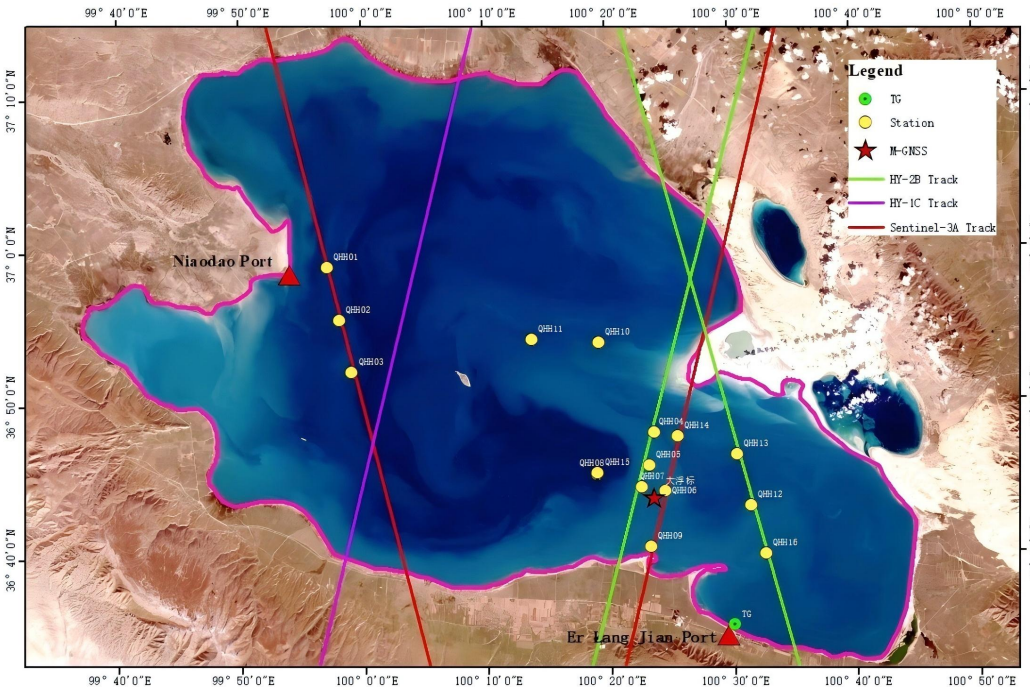


Figure 1. Schematic of the Qinghai Lake experimental site in 2019 (the green circle with * indicate tide gauge installation points; and the red triangle denote GPS reference station locations).

The in situ measurement data for this study were primarily collected during the Qinghai Lake experiment conducted from July to September 2019. A schematic diagram of the experimental sites is shown in Figure 1, in which the lines represent the satellite ground tracks. The oceanographic satellites passing over Qinghai Lake include the HY-1C satellite (purple line), the HY-2B satellite (green line), and the Sentinel-3A satellite (red line). To facilitate satellite altimeter research for lake surface height inversion, the experiment was designed to include high-precision GPS buoy measurements and geodetic height measurements at the satellite nadir points. The Sentinel-3A satellite has two tracks over Qinghai Lake: one ascending pass (67) and one descending pass (332). The 332 pass is located near the Erlangjian port, as shown by the red triangle in Figure 1. Due to the satellite altimeter footprint typically covering 5 to 7 km, and the correction radiometer providing wet atmospheric path delay with a footprint of approximately 25 km, the effective measurement data from the satellite altimeter over Qinghai Lake consist of about 3 to 5 points (as indicated by the dots in Figure 1). When observing lake surface heights with satellite altimeters, it is important to note that the nadir points of the altimeter do not exactly overlap with each cycle, and Sentinel-3A provides at least 3 to 5 s of valid observation data when passing over Qinghai Lake. To unify lake surface heights measured at different sub-satellite points within the same cycle, as well as those from different cycles, this study employs a normalization method. This method deduces the observed lake surface height at the satellite nadir points to a fixed reference point. By doing so, it enables the consistent representation of lake surface heights across different nadir points within a single cycle and standardizes the lake surface heights observed across different cycles. This approach supports accurate and long-term monitoring of lake surface height.

To implement this method, an experiment was designed using GPS buoy to measure the geodetic height differences between the satellite nadir points and a reference point (near Erlangjian port). The sea surface height measurement capability of the GPS buoy has been validated, and its accuracy meets the requirements for satellite altimeter calibration [43,44]. However, the ability of GPS buoy to measure lake surface height in high-altitude region has not been assessed. Therefore, the Qinghai Lake experiment was conducted in three phases: first, evaluating the ability of GPS buoy to measure lake surface height; second, using the GPS buoy to measure the geoid heights of the satellite nadir points and the reference point; third, analyzing the impact of each correction term and developing an algorithm for inverting the lake surface height from the altimeter data; and finally, applying various methods to extract valid lake surface height data from the satellite altimeter measurements.

2.1.1. GPS Buoy and Tide Gauge Comparison Experiment

Before using the Sentinel-3A altimeter to invert lake surface height, it is essential to obtain geoid data for Qinghai Lake. In this study, a GPS buoy measuring system was employed to measure the geoid at the nadir points (indicated by yellow circles in Figure 1) where the satellite passes over Qinghai Lake. To verify the measurement accuracy of the GPS buoy for lake surface height, a comparison experiment was conducted using tide gauge data to assess the height measurement capability of the GPS buoy measuring system. To ensure the accuracy of the water level observed by the tide gauge, the tide gauge was sent to a testing agency for accuracy assessment before the trial, and the results showed that the accuracy of the tide gauge used was better than 0.5 cm.

A tide gauge near Erlangjian port was used for precision evaluation of the GPS buoy measuring system, providing crucial data for subsequent GPS buoy geoid measurements. For detailed information on the methodology used to assess the precision of the GPS buoy measuring system with tide gauge data, refer to [10,45,46]. This paper focuses on the

implementation steps. First, a GPS reference station (GPSRS) was established at Erlangjian port, and the instrument was required to be kept level during its setup.



Figure 2. Establishment of GPS reference station.

Next, the tide gauge was affixed to the centering rod, and the height from the tide gauge sensor to the top of the centering rod was measured, ensuring that the centering rod remained level (as shown in Figure 3).



Figure 3. Diagram of the installation of the tide gauge on the centering rod in an erect position (the red circle is level bubble, which indicates the centralization of the centering rod).

Finally, GPS buoy was deployed near the tide gauge. Depending on the field conditions, the moored GPS buoys were attached to the test vessel or secured to the shore and placed approximately 10 m away from the stern of the vessel or the shore to ensure that the GPS measurements were not affected by other factors. In order to ensure the validity of the GPS buoy measurement data, the deployment time of the GPS buoy is no less than 6 h.

After deploying the GPS buoy and before retrieval, the height difference from the GPS reference station (GPSRS) to the top of the centering rod was measured twice using a leveling instrument. Depending on field conditions, the leveling instrument was used to link specific landmarks on the shore with the GPSRS, and a ruler was employed to measure the height from the water surface to these landmarks. The absolute benchmark of the tide gauge was then determined, and the consistency between the lake surface height measurements obtained from the tide gauge and the GPS buoy was analyzed.

2.1.2. Geoid Height Measurement Experiment

In the algorithm for satellite altimeter inversion of lake surface height, it is essential to determine the geoid differences between the tide gauge location and the satellite nadir points. This study measures the geoid at twelve nadir points of the HY-2B and Sentinel-3A satellites over Qinghai Lake (indicated by the yellow dots in Figure 1), establishing a connection between the geoid at the tide gauge location (represented by the green circles in Figure 1) and the nadir points.

The specific experimental steps are as follows:

1. Deploy a moored GPS buoy from the measurement vessel, positioning it approximately 30 m behind the stern to minimize interference from the vessel's hull. The GPS buoy should continuously record measurements for no less than 1 h;
2. During the experimental period, the tide gauge at Erlangjian port operates normally, recording changes in the water level of Qinghai Lake. Simultaneously, the GPS reference station (GPSRS) operates normally, providing reference data for the dynamic solution of the GPS buoy throughout the experiment.



Figure 4. Deployment strategy for the GPS buoy.

These measurements provide the necessary geoid differences for the altimeter inversion of lake surface height.

2.2. Data Introduction

This study employs the SAR altimeter data to investigate the variations in lake surface height of Qinghai Lake. The primary data utilized in this research include Sentinel-3A SRAL data, tide gauge observational data, GPS buoy, and GPSRS observational data.

2.2.1. Sentinel-3A SRAL Data

This study uses inland water data from the Sentinel-3A SRAL to monitor the water level changes in Qinghai Lake. Previous studies on the lake's water levels have utilized data from satellites such as ENVISAT, ICESat, Cryosat-2, Jason-1, and Jason-2 for precise calculations and analyses. Although the orbits of these satellites pass over the Qinghai Lake basin, the relatively large footprint (5–7 km) of traditional satellite altimeters, coupled with the transition from land to water as the satellites pass over lakes, causes a 3–5 s modality switch impact. This results in a limited amount of effective data from traditional satellites over lakes. In contrast, the Sentinel-3A, launched in February 2016, represents a new generation of radar altimetry missions. It is equipped with a dual-frequency (Ku and C-band) Synthetic Aperture Radar Altimeter (SRAL) and is the first to offer global coverage in Synthetic Aperture Radar (SAR) mode with finer along-track resolution. The dual-frequency SRAL uses delay-Doppler technology, which, compared to traditional satellite altimeters, enhances the along-track resolution (with a footprint of approximately

330 m). This improvement enables more effective measurements over lakes and enhances the capability of satellite altimeters for lake level monitoring [41].

The Sentinel-3A Surface Topography Mission is jointly operated by the European Space Agency (ESA) and the European Organization for the Exploitation of Meteorological Satellites (EUMETSAT), providing operational observation services for land and sea surfaces. ESA is responsible for producing Level-2 products for inland water bodies, while EUMETSAT handles Level-2 products for the ocean, including coastal areas. For inland water observation, users are encouraged to use Land Level-2 products. This study focuses on lake surface height measurements and therefore employs the Land Level-2 data published by ESA. The data used in this study are from version 005 (Baseline Collection 005), released by ESA in September 2023. The ESA Land Level-2 product includes three types of data.

To study the water level changes in Qinghai Lake, we used the SR_2_LAN_HY data from version 005 (Baseline Collection 005), as shown in Table 1, row 1. Consistent with version 004 and earlier, version 005 also includes two NetCDF data files: standard_measurement.nc and enhanced_measurement.nc.

Table 1. Sentinel-3A Land Level-2 products.

Data Name	Data Type	Measurement Range
SR_2_LAN_HY	Hydrology Thematic Products	Surface topography estimations of lakes and rivers
SR_2_LAN_SI	Sea Ice Thematic Products	Estimations of the radar freeboard over the Arctic and Antarctic sea ice
SR_2_LAN_LI	Land Ice Thematic Products	Surface topography estimations of the Greenland and Antarctic ice sheets

The standard_measurement.nc data file primarily contains geophysical parameters extracted from the waveform data, along with instrumental correction parameters needed for altimeter range data correction, as well as other relevant parameters. The *enhanced_measurement.nc* file includes all parameters from the *standard_measurement.nc* file, along with additional data such as the altimeter waveform, geophysical and time data, microwave radiometer (MWR) brightness temperatures, instrumental corrections, delay-Doppler stack parameters, and more [42].

Unlike versions 004 and earlier, version 005 introduces significant changes to the data format. The *enhanced_measurement.nc* data file now includes 20 Hz range data for longitude, latitude, and altitude, as well as ionospheric corrections. However, corrections for dry and wet atmospheric effects, sea state bias, and tidal effects (including ocean tide, load tide, solid earth tide, and pole tide) are still provided at 1 Hz. Additionally, the *num_20hz_meas_01_ku* parameter, which is essential for converting 1 Hz data to 20 Hz, is included. Since this study requires the use of 20 Hz altimeter data to invert lake water levels, the 1 Hz correction data must be converted to 20 Hz prior to calculating the lake water levels.

This paper uses the data of 97 cycles from the 001 cycle from the launch of Sentinel-3A in 2016 to May 2023, more than seven years of data, to study the changes in the water level of Qinghai Lake.

2.2.2. Tide Gauge Data

Tide gauges measure changes in water level from the sensor to the lake's surface (denoted as h in Section 2.3.2, and Equation (5)). Since a pressure-type tide gauge is used, variations in atmospheric pressure can affect the measurement data, particularly at altitudes above 3000 m, such as the location of Qinghai Lake. Therefore, barometric

pressure correction is necessary before converting the data to lake surface height. The altitude at Erlangjian port, located near Qinghai Lake, is approximately 3200 m, resulting in an atmospheric pressure of about 0.69×10^5 Pa, which is considerably lower than the standard atmospheric pressure of 1.013×10^5 Pa.

The pressure-type tide gauge is calibrated with standard atmospheric pressure. Therefore, at the high-altitude location of Qinghai Lake, where the atmospheric pressure (P) is 0.69×10^5 Pa, the corresponding water level (h measured by the tide gauge using the hydrostatic pressure formula (Equation (1)) is approximately -3.29 m.

$$P = \rho g h \tag{1}$$

In the formula:

- P represents atmospheric pressure, measured in Pascals (Pa);
- ρ represents the density of water, approximately 1.0×10^3 kg/m^3;
- g represents the acceleration due to gravity, approximately 9.8 N/kg;
- h represents the height of the water level change due to pressure, measured in meters (m).

To correct the water level data measured by the pressure tide gauge for atmospheric pressure, another pressure tide gauge of the same model is installed above the water surface near the submerged tide gauge. The data from the above-water pressure tide gauge are then used to correct for atmospheric pressure. This approach has the advantage over directly using atmospheric pressure data from a meteorological station, as it avoids errors associated with inconsistencies in the parameters of Equation (1), such as the choice of standard atmospheric pressure (P) and the acceleration due to gravity (g).

Figure 5 shows the data measured by the pressure tide gauge installed on the shore. From Figure 6, it is evident that during the experimental period from June to September 2019, variations in atmospheric pressure led to an average water level change of approximately -3.155 m, which closely matches the -3.29 m value obtained through a simple calculation using Equation (1). This further confirms the superiority of the method involving the direct installation of a pressure tide gauge of the same model. Additionally, from Figure 6, the standard deviation (STD) of the water level data inverted from the pressure tide gauge above the water was calculated to be 0.036 m. This indicates that the overall water level change due to atmospheric pressure is 3.6 cm, while the difference between the maximum and minimum values reaches 25–30 cm. This suggests that accurate water level measurements can only be obtained by applying atmospheric pressure corrections when using a pressure tide gauge.

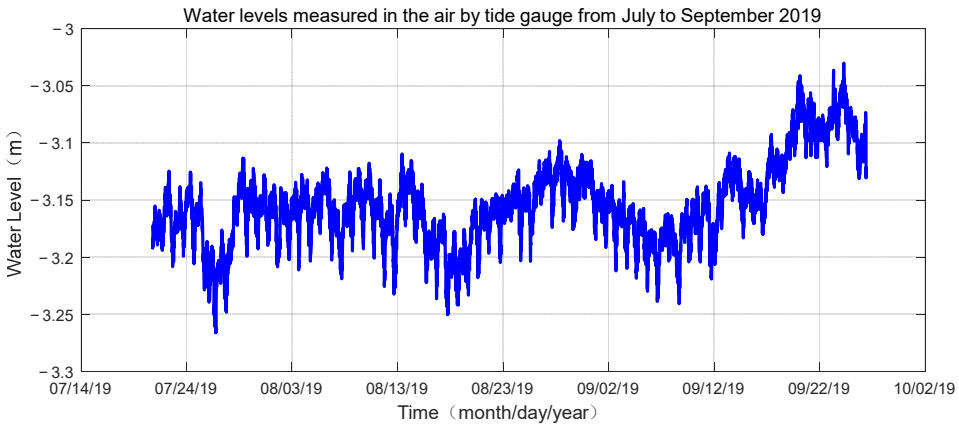


Figure 5. Water level data measured by the pressure tide gauge installed in the air.

After correcting the water level data measured by the atmospheric pressure from the pressure tide gauge above the water, the data must be converted into lake surface height based on the reference ellipsoid, as described in Section 2.3.2 using Equation (5). To ensure consistency across the satellite altimeter, tide gauge, and GPS buoy measuring system data, we select the reference ellipsoid used by the Sentinel-3A satellite altimeter as the unified benchmark. This ellipsoid has a semi-major axis of 6,378,137 m and an eccentricity of 0.0033528.

2.2.3. GPS Buoy and GPSRS Data

The GPS buoy measuring system is primarily used to determine the elevation of the lake surface relative to the reference ellipsoid, i.e., the lake surface elevation. In this study, the data from the GPS buoy measuring system serve two main purposes: (1) to validate measurements obtained from the tide gauge and (2) to collect geoid data at Qinghai Lake. The system consists of two key components: the GPS buoy (Figure 4) and the GPS receiver station (GPSRS) (Figure 2). The principle behind the GPS buoy measuring system is the use of a long-term stable GPS benchmark station to provide an absolute reference for the buoy. The lake surface height measured by the system is derived through dynamic processing of the buoy data [43,44,46]. Detailed data processing methods for the GPS measuring system in this experiment are provided in Section 2.1 of Zhai (2022) [46]; this paper offers only a brief overview.

During the experimental period, the GPSRS operated continuously from 13 June to 24 September 2019. It was located on the rooftop of a hotel approximately 500 m from the tide gauge setup (marked by a red triangle in Figure 1). The system utilized a South Net S9 receiver and an STHCR3-G3 antenna, with a reception frequency of 1 Hz, enabling kinematic processing of the GPS buoy data. The absolute coordinate solution for the GPSRS was obtained using GAMIT/GLOBK software (Release.10.4) developed by Massachusetts Institute of Technology (MIT) and the Scripps Institution of Oceanography at the University of California, San Diego, CA, USA. This software provides high-precision GPS positioning and orbit determination, with long baseline solution accuracy reaching 10^{-9} and absolute height precision for single-day static GPS station solutions better than 1.5 cm [47,48]. The GPS buoy data were processed using dynamic GPS methods, primarily employing the Track module of GAMIT/GLOBK software, which integrates precise ephemerides and raw observation data in RINEX format [49].

2.3. Lake Surface Height Data Processing Methods

Water level variation is a key parameter for studying the environmental impacts and responses of lakes. Traditional methods rely on water level data collected at hydrological stations to monitor changes in lake water levels. These data are typically referenced to a specific benchmark point, and the accuracy of the measurements is influenced by the uniformity and stability of this benchmark. In line with the definition of sea surface height, we define lake surface height as the elevation of the lake surface relative to the reference ellipsoid. Using lake surface height provides a reliable means to represent lake water levels, with the reference ellipsoid serving as a globally recognized benchmark used by satellite altimeters. This approach offers a consistent and standardized reference for multi-satellite observations of lake water levels and enables the creation of long-term datasets that can be compared with future satellite altimeter data. In this study, lake surface water levels are measured using data from tide gauges, satellite altimeters, and the GPS buoy measuring system.

2.3.1. Lake Surface Height Inversion Algorithm for Satellite Altimeter

Lake water level refers to the elevation of the free surface of a lake above a specified reference surface at a given time and location. As a dynamic free surface, the water level fluctuates in response to variations in precipitation and evaporation. The principle behind using satellite altimeters to measure lake water levels is analogous to that used for measuring sea surface height. The measurement process begins with the basic satellite principle, which involves subtracting the satellite altimeter's range measurement (after applying delay corrections) from the satellite's altitude relative to the reference ellipsoid (determined through precise orbit calculations). This yields the height of the lake surface relative to the reference ellipsoid. The formula for calculating sea surface height, as shown in Equation (2) [7–10], follows this same methodology.

$$SSH = h_{Alt} - h_{range} - \sum Cor \quad (2)$$

The satellite altimeter measures the distance from the satellite to the sea surface (denoted as h_{range}) by receiving the echo of the emitted pulse. This pulse is influenced by several factors as it passes through the atmosphere and ionosphere. Taking into account instrumental errors, atmospheric refraction, sea state bias, and necessary geophysical corrections, the error can be derived using Formula (3) as follows:

$$\sum Cor = E_{Dry} + E_{Wet} + E_{Ion} + E_{SSB} + E_{Sol} + E_{Pol} + E_{load} + E_{oce} + E_{IB} + E_{hf} \quad (3)$$

In the formula:

- h_{Alt}—Orbital elevation of the satellite relative to the reference ellipsoid;
- h_{range}—Distance measured by the altimeter, specifically the distance from the satellite's pulse receiver to the water's surface;
- E_{Dry}—Dry tropospheric correction, which compensates for refraction errors caused by dry atmospheric conditions as the pulse passes through the troposphere;
- E_{Wet}—Wet tropospheric correction, accounting for delays in the pulse signal due to water vapor and moisture in clouds as the pulse traverses the troposphere. This correction is typically derived using atmospheric models or radiometer measurements;
- E_{Ion}—Ionospheric correction, which compensates for refraction errors caused by free electrons in the ionosphere. This is crucial for accurate satellite-to-sea surface distance calculations and is typically applied using global ionosphere models (GIMs) and measurements from dual-frequency altimeters [10];
- E_{SSB}—Sea state bias correction, which compensates for errors due to the offset of the echo center towards the trough of ocean waves. Since fewer echo pulses are scattered at the wave trough than at the crest, this results in a shift in the echo center, and consequently, a shift in the calculated sea surface position;
- E_{Sol}—Solid tide correction, which compensates for errors arising from solid Earth deformations caused by gravitational forces from the Sun and the Moon;
- E_{Pol}—Pole tide correction, which compensates for errors due to the elastic response of the Earth's crust to shifts in the orientation of the Earth's rotational axis, causing surface changes;
- E_{load}—Loading tide correction, which accounts for errors due to solid Earth deformations resulting from tidal forces exerted by the ocean;
- E_{oce}—Ocean tide correction, which compensates for errors due to variations in the rise and fall of ocean tides;
- E_{IB}—Inverse barometric correction, which adjusts for errors caused by changes in atmospheric pressure at the sea surface, affecting sea level rise or fall;

- E_{hf}—High-frequency response correction for atmospheric pressure and wind, which addresses errors in sea surface height caused by fluctuations in atmospheric pressure and wind, supplementing the inverse barometric correction.

Based on the sea surface height inversion formulas, Formulas (2) and (3), for satellite altimeters, we examine the specific challenges of measuring lake surface height using satellite altimetry and establish a more reasonable lake height inversion algorithm. This analysis primarily focuses on the tidal correction terms, sea state bias, and the influence of loading tides.

Tide Correction Analysis

Using in situ data from the tide gauge, we analyzed the presence of a tidal signal in Qinghai Lake. We selected the 24 h water level data recorded by the tide gauge on 15 July 2019 and present the results in Figure 6 below.

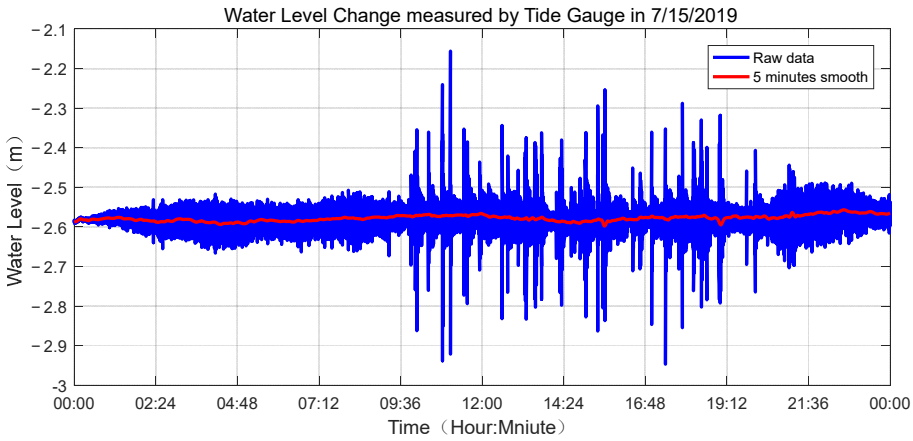


Figure 6. Tide gauge measurement of water level changes in Qinghai Lake on 15 July 2019.

The 1 Hz data from the tide gauge (blue line in Figure 6) cannot detect tidal signals, necessitating further processing. A data smoothing algorithm is applied to eliminate the impact of spikes. These spikes are primarily caused by the presence of a yacht dock at the Erlangjian port on Qinghai Lake. As shown in the plot, from 8 a.m. to 7 p.m., the yachts generate relatively regular water level fluctuations. To remove these high-frequency spikes without affecting low-frequency phenomena, such as tides, a 5 min low-pass filtering method is used. This approach effectively filters out high-frequency noise while preserving tidal signals, as it does not alter their period. After applying the 5 min low-pass filter, as indicated by the red line in Figure 6, it becomes evident that the daily water level variation in Qinghai Lake is minimal, with a standard deviation (StD) of approximately 0.8 cm. The changes caused by tides are negligible. Given that inland lakes, in contrast to oceans, have smaller areas, the tidal-induced water level fluctuations are minimal. Therefore, the tidal signal does not need to be considered in the satellite altimeter-based lake surface height inversion algorithm.

Sea State Bias Analysis

Based on Equation (3), we analyze the impact of sea state bias (SSB) on the lake surface height inversion algorithm for inland water bodies. Unlike oceans, lakes generally have smaller waves, with most having a height of less than 0.5 m. Currently, the sea state bias correction is based on significant wave height and wind speed derived from altimeter echo waveform inversion. However, for inland lakes, the waveforms differ substantially from those of the ocean, leading to significant errors in the inversion of wave height and wind speed measurements. Using the oceanic method for sea state bias correction

would therefore introduce considerable errors, compromising the accuracy of the results. Consequently, in the lake surface height inversion algorithm developed in this study, sea state bias is not considered for the time being.

Load Tide Analysis

Loading tide is included within the ocean tide. It refers to the Earth's response to the ocean tides, atmospheric tides, and solid tides caused by the gravitational pull of the sun and the moon, as observed from the ground. These tidal forces can cause deformations in the solid Earth. Loading tides specifically refer to the Earth's response to vertical displacements caused by the pressure exerted by marine and atmospheric tides on the land, with deviations typically within 2 cm. Similar to solid tide, the altimeter range data (h_{range}) include signals from loading tide. However, for lakes—being relatively small in size compared to oceans and exhibiting negligible tidal changes—the loading tide correction term can be neglected in the lake surface height inversion algorithm developed in this study.

Establishment of the Inversion Algorithm

Based on the satellite altimeter sea surface height inversion formulas, Formulas (2) and (3), we primarily analyzed the tidal correction term (E_{oce}), sea state bias correction term (E_{SSB}), and loading tide correction term (E_{load}). Given the specific characteristics of inland lakes, we found that these three correction terms are not relevant for error correction in inland water bodies. As for the polar tide (E_{Pol}) and solid tide (E_{Sol}), these terms have already been accounted for in GPS solutions. Therefore, when inverting lake surface height using satellite altimetry, it is necessary to subtract these two parameters accordingly.

Based on the comprehensive analysis, a more reasonable lake height inversion algorithm established using altimeter data is presented in Equation (4) as follows:

$$LakeH_{alt} = h_{Alt} - h_{range} - E_{Dry} - E_{Wet} - E_{Ion} - E_{Sol} - E_{Pol} - E_{IB} - E_{hf} \quad (4)$$

By utilizing the non-time-restricted (NTC) LAN Level 2 data from the Sentinel-3A SRAL and selecting in situ water level data from the tide gauge, we concluded that the tidal correction term can be neglected in the water level inversion for Qinghai Lake. The study analyzed the tidal correction terms, sea state bias, and the impact of loading tides and established a more reasonable lake height inversion algorithm for inverting lake surface height from satellite altimeter data.

2.3.2. Lake Surface Height Inversion Algorithm for Tide Gauge

The tide gauge used is an RBR pressure-type device, configured to collect data at a 1 Hz observation frequency to monitor real-time changes in lake water levels. It was installed at Erlangjian Port (indicated by the green dot in Figure 1), with a GPS reference station (GPSRS) located nearby. The tide gauge measures the water level changes from the sensor to the lake's surface (denoted as h in Figure 7 and Equation (5)).

Figure 7 presents a schematic diagram of the tide gauge used to observe lake surface height. The GPSRS provides the height from the tide gauge sensor to the reference ellipsoid (denoted as $H - h_1$ in the formula). Using Equation (5), the water level change data collected by the tide gauge for Qinghai Lake are inverted to derive the lake surface height.

$$H_{lake_TG} = H - h_1 + h \quad (5)$$

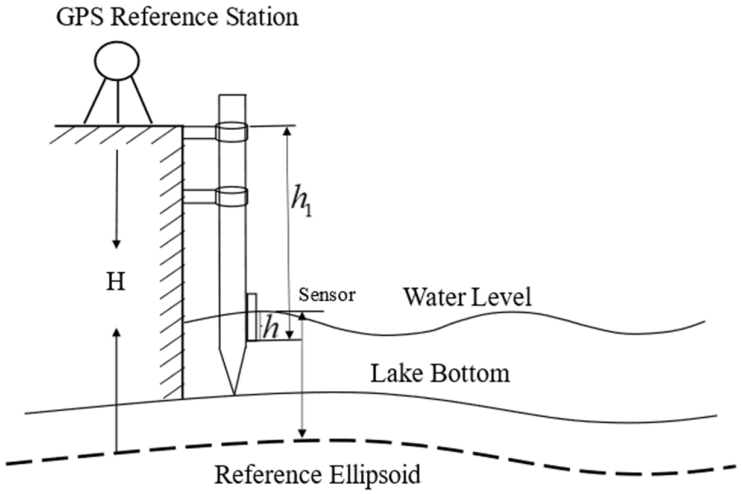


Figure 7. Schematic diagram of the method for measuring lake surface height with a pressure-type tide gauge.

3. Results

3.1. Precision of Lake Measurement with GPS Buoys

The elevation measurement capability of the GPS buoy measuring system is assessed using a pressure-type tide gauge. The data from the pressure tide gauge are processed with the lake surface height inversion algorithm described in Section 2.3.2 to determine the lake surface height, measured by the tide gauge, under the same reference ellipsoid as the GPS buoy.

This study uses a tide gauge to perform comparative tests with a GPS buoy, evaluating the measurement accuracy of the GPS buoy measuring system in high-altitude lakes. Two comparative tests were conducted with the tide gauge, and the results are presented in Figures 8 and 9. The first test, conducted on 14 July 2019 (shown in Figure 8), involved both the tide gauge and the GPS buoy operating at a measurement frequency of 1 Hz. Over a duration of approximately 3 h, the standard deviation (StD) between the two systems was 1.28 cm.

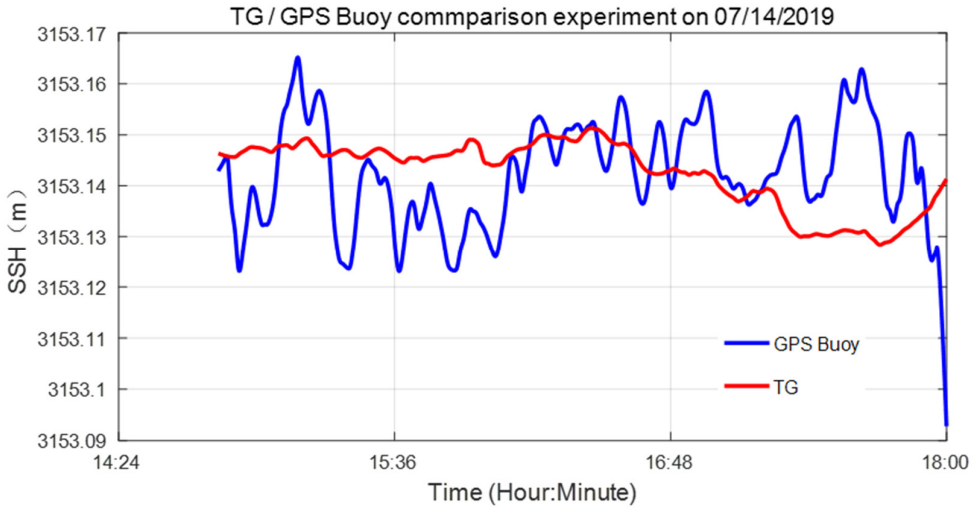


Figure 8. Results of the first comparative test between the tide gauge and GPS buoy.

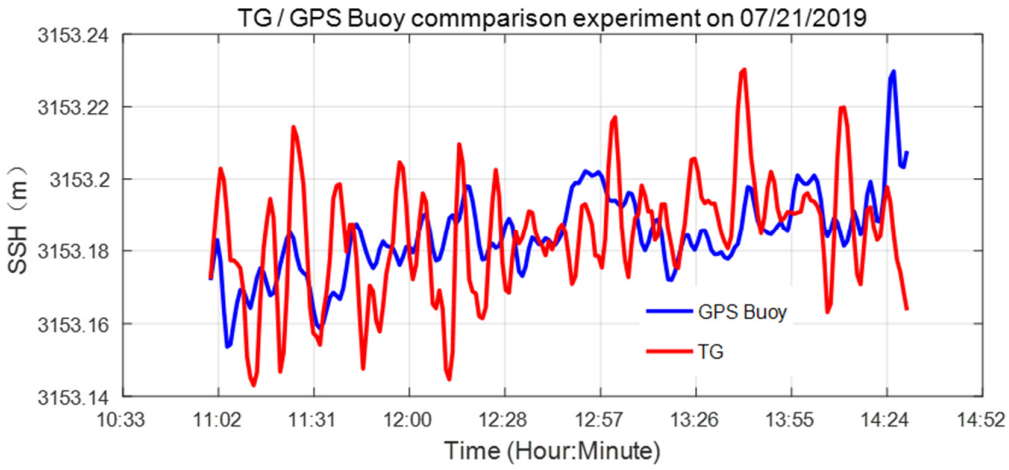


Figure 9. Results of the second comparative test between the tide gauge and GPS buoy.

The second comparative test was conducted from 11:00 to 14:30 on 21 July 2019, lasting approximately three and a half hours. Both the tide gauge and GPS buoy collected data at a frequency of 1 Hz, resulting in about 12,600 data points for each system. Due to the large volume of data, the measurements were averaged per minute before the comparison. The results, shown in Figure 9, depict the lake surface height measured by the GPS buoy (blue line) and the tide gauge (red line). The standard deviation (StD) between the two datasets was 1.18 cm.

An error analysis of the GPS buoy is discussed in detail in the literature [10,45,46]. Combining the results of the two comparative tests, the measurement accuracy of the GPS buoy in Qinghai Lake is approximately 1.23 cm, with the GPSRS located about 3 km away. Given that the measurement accuracy of satellite altimeters is around 3 cm [38,39,46], the accuracy of the GPS buoy meets the requirements for geoid measurements in Qinghai Lake.

3.2. Geoid Measurements of Qinghai Lake

This study employs normalization to invert the lake surface height from satellite altimeters over Qinghai Lake. Specifically, the observed lake surface height at the satellite's nadir point is extrapolated to the lake surface height at a fixed location. This method standardizes lake surface heights observed at different nadir points within a single cycle and also unifies measurements across multiple satellite cycles. The approach involves measuring the difference between the geoid at the satellite's nadir point and the shore, using this difference to extrapolate the satellite-derived lake surface heights to the tide gauge location on the shore.

Before conducting geoid measurements, it is essential to assess whether the water level changes in Qinghai Lake meet the requirements for measuring geoid undulation using the GPS buoy measurement system. The difference in lake surface elevation between the satellite's nadir point and the Erlangjian tide gauge, as measured by the GPS buoy system, is taken as the geoid undulation between the two points. A key prerequisite for this method is that the lake water level remains relatively stable during the measurement period, ensuring accuracy at the centimeter level. As shown in Figure 6 in Section Tide Correction Analysis, the 24 h continuous water level data from the tide gauge indicate that the daily variation in Qinghai Lake's water level is minimal, with a standard deviation (StD) of approximately 0.8 cm. Building on this, we further analyze the intra-hour changes in the lake's water level.

The water level changes in Qinghai Lake over a one-hour measurement period, as shown in the two measurements in Figure 10, are relatively small during both periods (the black curve in the figure represents the 5 min smoothed data), with a standard deviation

(StD) of less than 1 cm. This stability in the lake's water level provides a favorable condition for conducting GPS buoy measurements of the geoid.

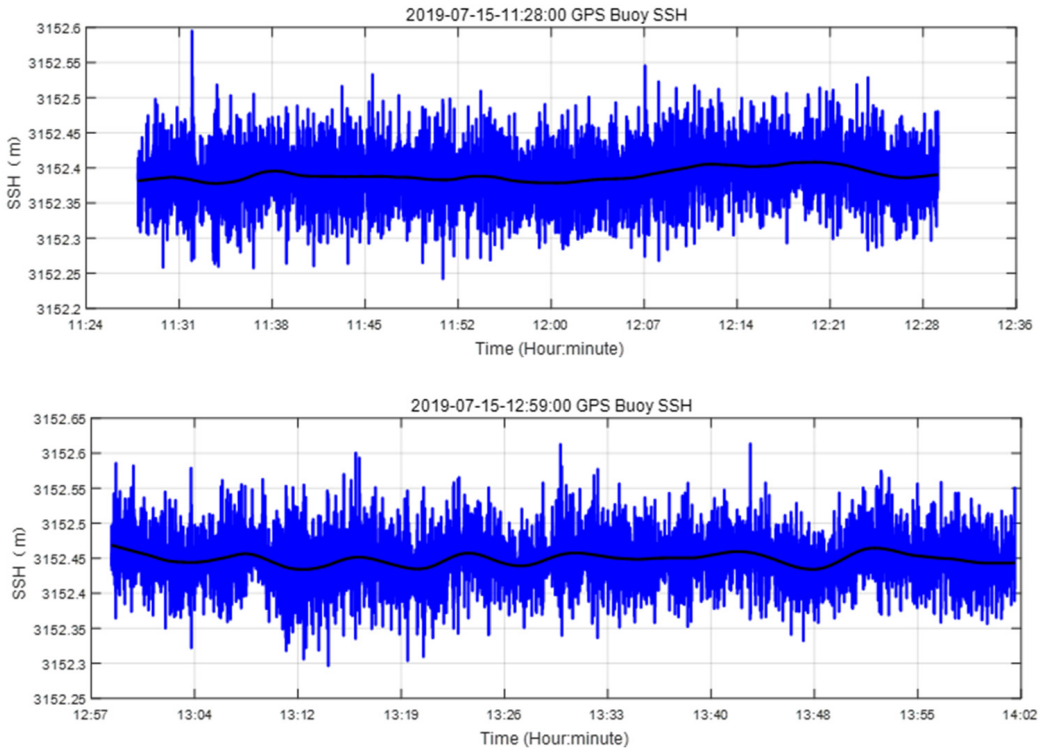


Figure 10. Variation in lake water level during geoid measurement on 15 July 2019.

During the geoid undulation measurement experiments, GPS buoys were deployed at each station by stopping the vessel (as shown in Figure 4) to measure continuously at each point for 1 h. We analyzed the lake water level changes during this period and used the standard deviation (StD) to characterize the variation in water level, as shown in Figure 11. Over the 18 measurements, the lake level exhibited minimal change, with an average StD of 1.05 cm. This suggests that the use of GPS buoys for single-point geoid measurements is feasible and can ensure the precision of the geoid data.

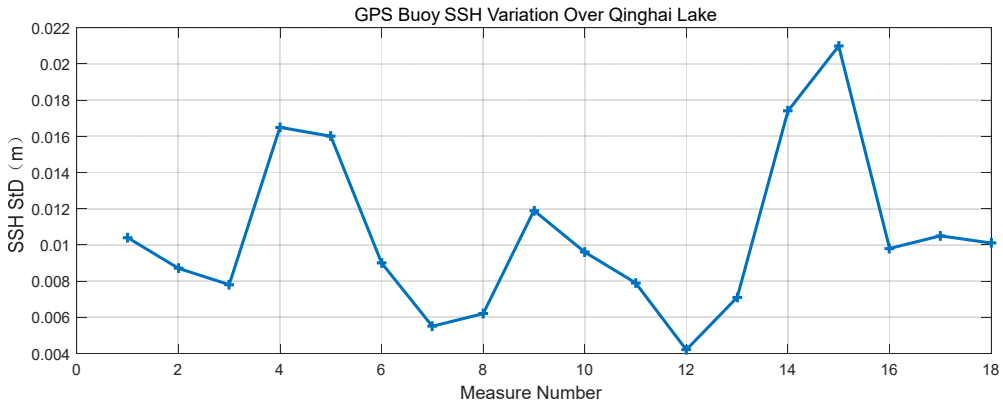


Figure 11. Variation in lake water level during geoid measurement in July 2019.

The original plan was to complete geoid measurements at 12 satellite altimeter footprints; however, the actual measurements were conducted at 18 geoid points. The latitude and longitude coordinates of the Sentinel-3A satellite altimeter footprints over Qinghai Lake are provided in Table 2.

Table 2. Coordinates of geoid measurement points.

Sentinel-3A (Ascending Orbit 67)	Longitude (°E)	Latitude (°N)
QHH01	99.9481	36.9864
QHH02	99.9662	36.9279
QHH03	99.9843	36.8694
Sentinel-3A (Descending Orbit 332)	**Longitude (°E)**	**Latitude (°N)**
QHH14	100.4254	36.7954
QHH06	100.4074	36.7369
QHH09	100.3894	36.6783

3.3. Normalized Lake Surface Height

In Section 2.3.1, we presented the satellite-altimeter-based algorithm for inverting lake surface height and applied it to Sentinel-3A SRAL data. Given that the 67-pass orbit provides more ground track points over Qinghai Lake than the 332-pass orbit (as shown in Figure 1, with red lines indicating the 67-pass orbit near Northwest Qinghai Lake), this study uses data from the ascending orbit of Sentinel-3A (067 pass) to analyze variations in the lake's surface height. Satellite altimeters make observations by the echo of the pulses they transmit. Therefore, when a satellite altimeter is used for lake measurements, some of the satellite data at the sub-satellite points will be affected by the land. When processing the satellite altimeter data of Qinghai Lake, the first step is to obtain the satellite data that is not affected by the land and then effectively extract the data through further analysis. Using the satellite altimeter lake surface height inversion formula (Equation (4)), the results are illustrated in Figure 12 below.

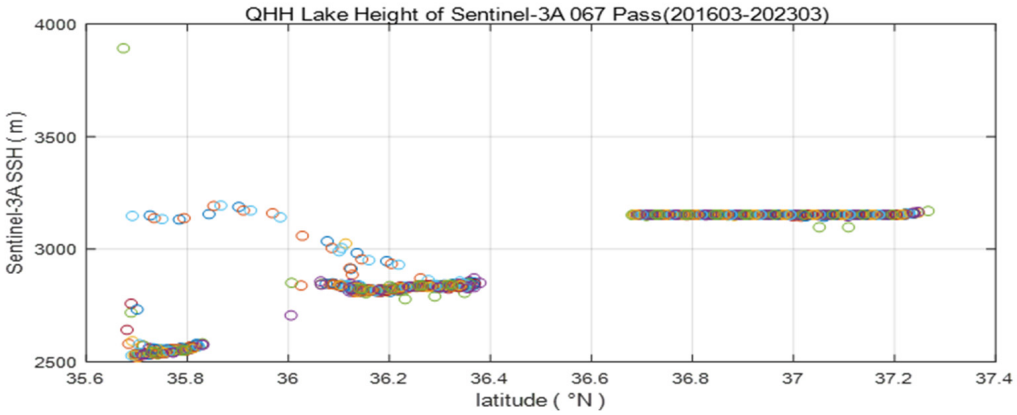


Figure 12. Distribution of Qinghai Lake water surface height derived from Sentinel-3A 067 pass with latitude.

Figure 12 shows that the lake surface height of Qinghai Lake, as measured by the satellite altimeter, follows a three-segment distribution with latitude. The different colors in Figure 12 represent different cycle data, and the same for Figures 13 and 14. The segment between 36.7°N and 37.2°N is notably stable and continuous. Therefore, the initial step in developing an effective extraction method is to apply regional filtering.

3.3.1. Regional Filtering

First, we collected the inverted lake surface height data from cycles 01 to 97 within the region bounded by 36.8°N to 37.1°N, then zoomed in for a more detailed analysis of the data variations, as shown in Figure 13. After applying regional filtering, noticeable data anomalies persist; however, the overall trend of the data changes is now clear. This also highlights the need for further data screening to remove these anomalies and eliminate gross errors.

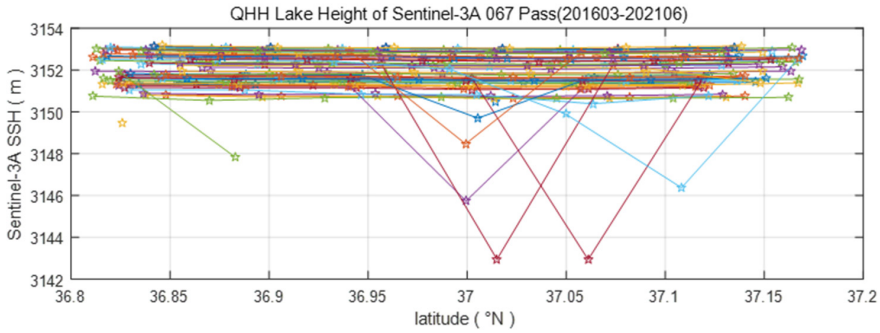


Figure 13. Variations in lake surface height of Qinghai Lake derived from Sentinel-3A 067 pass after regional screening.

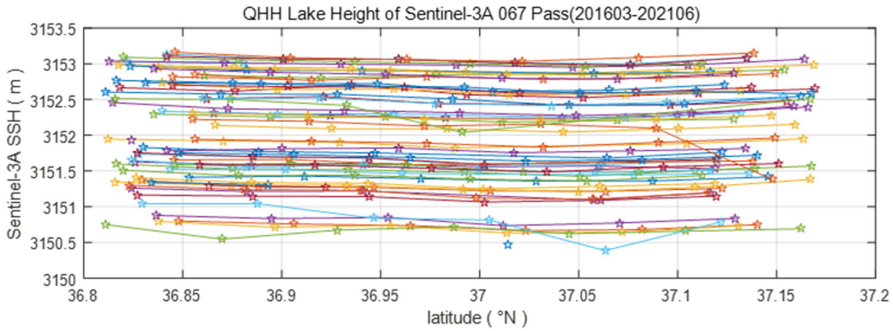


Figure 14. Variations in lake surface height of Qinghai Lake derived from Sentinel-3A after regional and threshold filtering.

3.3.2. Threshold Filtering

Based on the regional filtering results shown in Figure 13, anomalies are observed within a localized area, with some data points dipping between approximately 36.88°N and 37.11°N. This indicates the presence of gross errors that need to be addressed. To resolve this, a threshold filtering range was applied, with the vertical coordinate suggesting a range between 3150 and 3154 m. After removing the outliers, the filtered results are presented in Figure 14.

From Figure 14, it can be seen that after applying threshold filtering, the lake surface heights measured by the satellite altimeter become smoother and more concentrated. Following both regional and threshold filtering, we selected a longer time series for further analysis. Specifically, we applied regional and threshold filtering to the Sentinel-3A SRAL data of Qinghai Lake from March 2016 to May 2023. The data were then inverted and averaged per pass, allowing us to perform a time series and standard deviation analysis of the lake surface height. The results are presented in Figures 15 and 16.

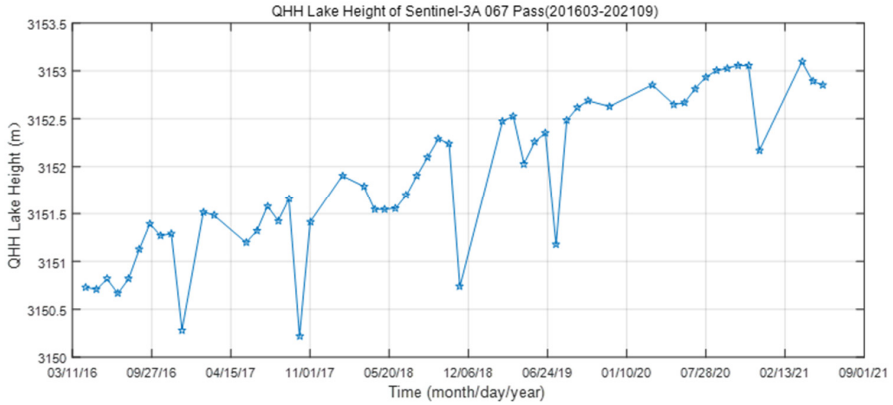


Figure 15. Time series of lake surface height derived from Sentinel-3A SRAL after regional and threshold filtering.

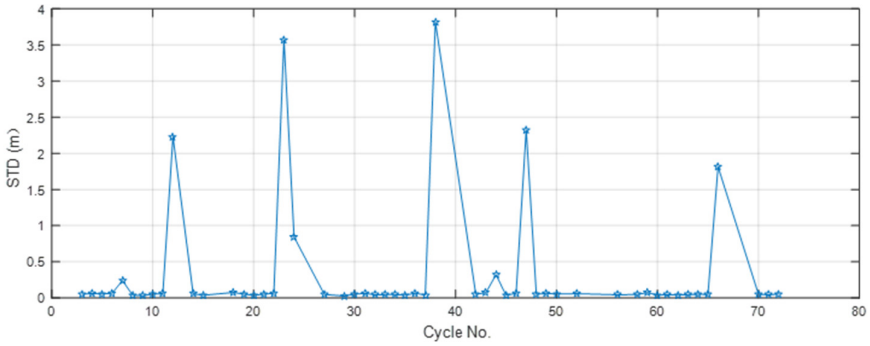


Figure 16. Single-pass standard deviation (StD) statistics of lake surface heights derived from Sentinel-3A SRAL after regional and threshold filtering.

By comparing Figures 15 and 16, we observe several notable data fluctuations. Specifically, five dips in the lake surface height data, identified as anomalies in Figure 15, correspond to five instances of larger standard deviations occurring at roughly the same times in Figure 16. This suggests a correlation between the lake surface height anomalies and variations in surface height within the same pass. To facilitate a comparative analysis, both datasets are presented on the same graph in Figure 17.

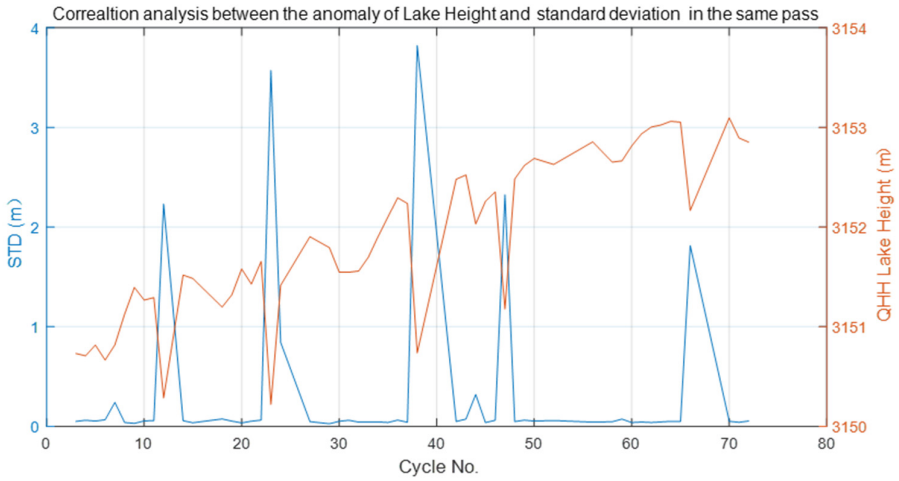


Figure 17. Comparative plot of the time series of lake surface heights and the standard deviation (StD) of lake surface height in the same pass.

Upon examining Figure 17, it is evident that the anomalies in lake surface height are caused by significant scatter in the data within the same pass. To refine the analysis, it is necessary to remove these anomalous lake surface height data points from Figure 15. This can be achieved by performing an anomaly analysis of the standard deviation (StD) values for each pass.

3.3.3. Altimeter Range Filtering

After two rounds of filtering, each satellite overpass contains multiple valid data points. Building on these initial filters, altimeter range filtering is then applied. The principle of this method is as follows: the 1 Hz range (h_{range}) data from the satellite altimeter are derived by averaging the 20 Hz range data. The standard deviation (StD) of these 20 range measurements is calculated and used as the filtering criterion. Data with a standard deviation greater than 0.2 m are considered anomalous, and the corresponding 1 Hz altimeter range data are removed. After applying regional and threshold filtering

to the data from March 2016 to May 2023, the altimeter range filtering was performed, resulting in the data shown in Figure 18.

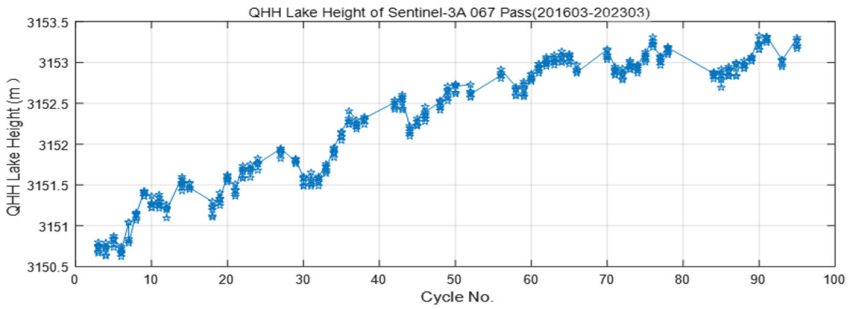


Figure 18. Time series of lake surface height derived from the improved and effective satellite altimeter extraction method for Qinghai Lake.

From Figure 18, it can be concluded that the improved lake surface height inversion algorithm, after applying the three filtering steps, effectively removes outliers. Additionally, Figure 18 shows an increasing trend in the water level of Qinghai Lake. Since each pass contains multiple valid data points (approximately 5–8 per pass), a vertical distribution of lake surface heights is observed in the figure (indicated by red circles). Direct averaging of these data points would introduce errors due to variations in both the number and positioning of valid data points. Consequently, further processing is necessary to refine the results.

3.3.4. Normalization of Lake Surface Height

In the previous sections, we developed a robust algorithm to invert the lake surface height (LSH) of Qinghai Lake, incorporating both the LSH inversion algorithm and the LSH data validation extraction method. This enables the derivation of lake surface heights from satellite altimeter data. Since each satellite pass over Qinghai Lake yields a varying number of valid data points across different cycles, it is essential to transform these surface heights to a common reference point using geoid undulation. The transformed heights are then averaged for each cycle to obtain the normalized lake surface height. The results are presented in Figure 19.

As shown in Figure 19a, the water level of Qinghai Lake has been steadily rising. By calculating the annual average values for 2016 and 2022, the rate of increase is determined to be 29.9 cm per year. Figure 19b illustrates that the residuals from 2021 to 2023 are predominantly negative, suggesting that the rate of water level rise between 2016 and 2020 was significantly higher than the rate observed from 2020 to 2023.

Table 3 summarizes the maximum, minimum, and average lake surface heights of Qinghai Lake from 2016 to 2023, along with the rate of the water level increase. The analysis reveals that the rate of the water level increase is 30 cm per year. Additionally, by subtracting the minimum value from the maximum value, it is found that the lake surface height rose by 2.41 m over the seven-year period.

Using the newly developed satellite altimeter inversion algorithm, we effectively processed the data and applied a three-step filtering approach, including regional selection, threshold filtering, and altimeter range selection, to eliminate anomalous data. The analysis of the Qinghai Lake data from March 2016 to May 2023 reveals a clear upward trend in the lake's water level over this seven-year period, with a total rise of 2.41 m, corresponding to an annual increase of 0.30 m per year.

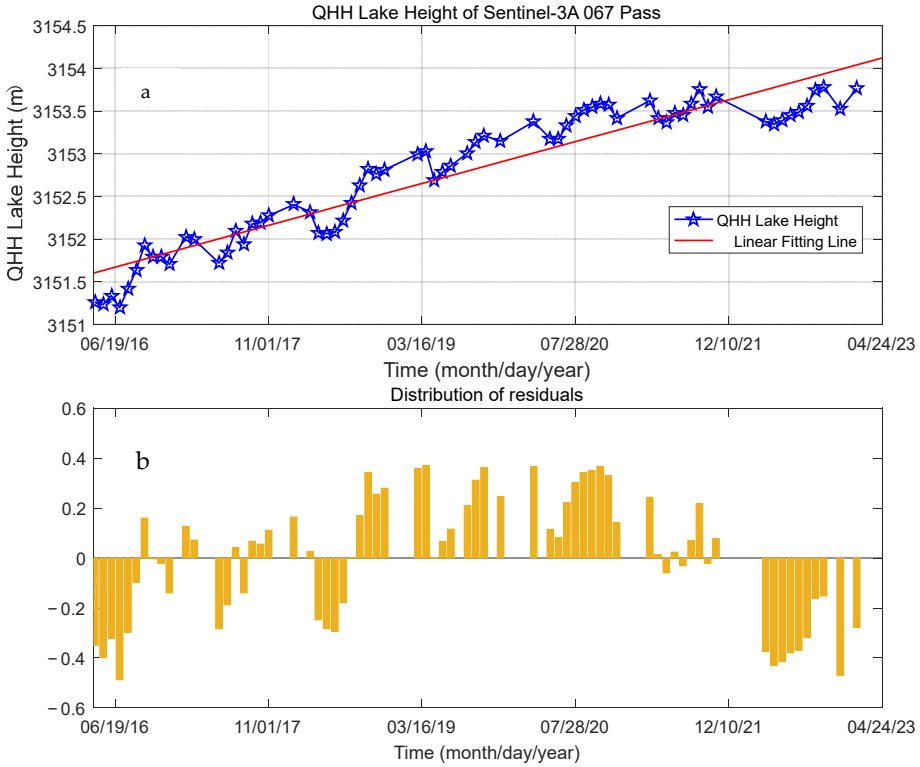


Figure 19. The normalized average lake surface height of Qinghai Lake obtained after normalization. (**a**) The rising trend of Qinghai Lake water level; (**b**) The distribution of residuals.

Table 3. Statistics on Qinghai Lake's lake surface height from March 2016 to May 2023.

Maximum Value	Minimum Value	Average Value	Rate of Increase
13,153.10 m	3150.69 m	3152.02 m	0.30 m/a

4. Discussion

This study utilized Sentinel-3A SRAL data from cycles 2 to 97, spanning from March 2016 to May 2023, to investigate the water level changes of Qinghai Lake. As shown in Figure 19a, the effective observation period for the lake surface height inversion using Sentinel-3A SRAL data began on 13 April 2016 and ended on 31 January 2023, corresponding to cycles 3 to 95. However, only 68 of these cycles met the criteria for effective data extraction, as Qinghai Lake, located at 37°N in a high-altitude region, has a frozen surface from December to March each year. During this period, the satellite altimeter measures the ice surface height, and in the latest version of the data used in this article, the SR_2_LAN_HY data from version 005 (Baseline Collection 005), as shown in Table 1, row 1, no satellite altimeter data are available for lake surface height.

The altimeter on the Sentinel-3A satellite has a height measurement accuracy of about 3 cm [38,39,44]. The geoid differences measured by GPS buoys are used to normalize the satellite data in this paper, so the error of the GPS buoys' measurements (1.23 cm) will be transferred to the lake surface height. Therefore, according to the error propagation algorithm, the final accuracy of the lake surface height inversion algorithm established in this article is about 3.24 cm.

The statistics in the fourth column of Table 4 for Sentinel-3A SRAL data reveal a consistent gap in the observations from December of each year to March of the following year. This pattern is consistent with the findings of Wang Guanxin (2020) [50], which show that lake ice begins to form in December and starts to melt in early March, based on in

situ ice thickness measurements from 1983 to 2018. Therefore, it can be concluded that the missing data are primarily due to the presence of ice, which interferes with the satellite altimeter's ability to obtain distance measurements.

Table 4. Monthly distribution of lake surface height for Qinghai Lake from March 2016 to May 2023.

Year	Month of Maximum Value	Month of Minimum Value	Months with Missing Data
2016	09	07	03/2016
2017	11	05	01/2017 and 12/2017
2018	09 and 11	05	02/2018 and 12/2018
2019	10	04	01/2019–02/2019 and 12/2019
2020	10	05	01/2020–02/2020 and 04/2020
2021	09	05	01/2021–02/2021 and 11/2021–12/2021
2022	10	05	01/2022–03/2022 and 11/2022

Figure 19a clearly shows that while the overall trend in Qinghai Lake's water level is upward, there are still seasonal fluctuations, following the pattern of rising, falling, and rising. The monthly distribution of Qinghai Lake's surface height (Table 4) reveals that the water level peaks in September and October, while it reaches its lowest point in April and May. Zhao Yun (2017) [44] analyzed Qinghai Lake's water level data from 2002 to 2015 and identified a clear seasonal variation, with the lowest levels occurring in May and the highest in September. Similarly, Jiang Weiping (2008) [51] analyzed monthly average water levels from hydrological stations between January 1984 and October 2005 and observed significant seasonal variations. These findings are consistent with the results of this study, which also identifies September and October as the months with the highest water levels, and April and May as the months with the lowest.

Li Ting (2016) [52] analyzed 40 years of average water level data (1974–2013) from hydrological stations around Qinghai Lake, spanning 480 months, in combination with remote sensing imagery. Li's analysis identified April as the dry period and September as the wet period for the lake. These findings are consistent with the seasonal water level variation observed in this study.

As discussed with the Qinghai Lake management department, no events affecting the rise in lake water levels, such as landslides, have occurred. The water level changes in Qinghai Lake are primarily influenced by precipitation. The region experiences its rainy season in July and August, which leads to increased runoff and results in the highest water levels in September and October. In contrast, during the winter months, low temperatures cause freezing and evaporation, leading to the lowest water levels in May. Research by G. Zhang et al. (2017) [21] indicates that precipitation is the most significant contributor to lake volume increases on the Tibetan Plateau, accounting for approximately 74%, followed by glacier melting (about 13%) and permafrost degradation (around 12%). Additional qualitative analyses [53,54], water balance model simulations for individual lake basins [55–57], and estimates of glacier mass loss contributions to increased lake volume [58,59] further support the conclusion that increased precipitation is a major driving factor behind lake expansion.

The analysis of Figure 19a clearly indicates a continuous rise in the water level of Qinghai Lake. By calculating the average values for 2016 and 2022, the annual increase is estimated at 30 cm. Figure 19b reveals a negative overall residual from 2021 to 2023,

suggesting that the rate of the water level increase between 2016 and 2020 was substantially higher than that observed from 2020 to 2023.

The water level increase of Qinghai Lake is analyzed in two distinct phases. As shown in Figure 20, from 2016 to 2020, the rate of increase was 47.2 cm per year (blue lines with star in Figure 20), while from 2020 to 2022, the rate nearly stagnated (blue lines with circle in Figure 20). Consequently, the linear regression line from 2016 to 2023, represented by the red line in Figure 20, yields an average rate of increase of 30 cm per year. These observations suggest that the water level changes of Qinghai Lake can be divided into two periods: from 2016 to 2020, with a rate of increase of 47.2 cm/year, and from 2020 to 2022, when the rate of increase dropped to 13 cm/year. Additionally, in 2022, the water level slightly decreased by 2 cm compared to 2021. Liu Jinxiu et al. (2021) [60], using HY-2B satellite altimeter data, reported a 45 cm rise in the water level of Qinghai Lake from 2019 to 2020. The Qinghai Hydrological Information Network recorded a water level of 3195.98 m on July 1, 2019 and 3196.35 m on 1 July 2020, indicating a rise of 37 cm within one year. In this study, the calculated rise from July 2019 to July 2020 was 43 cm, further confirming the reliability of the calculated rate of increase for Qinghai Lake.

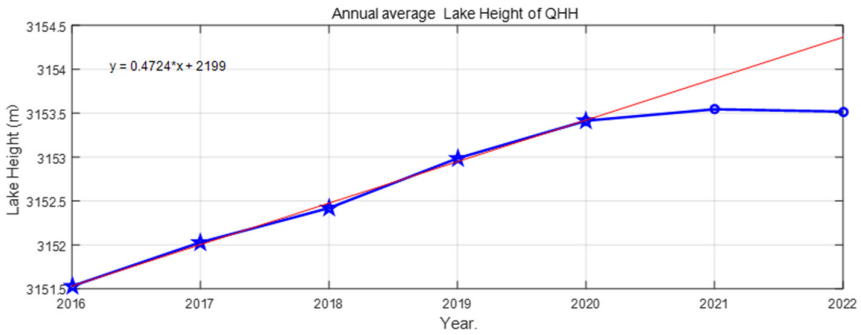


Figure 20. Distribution of annual average lake surface height changes of Qinghai Lake.

5. Conclusions

With the ongoing improvements in satellite altimeter precision, these instruments are increasingly being employed to monitor inland water bodies. The Sentinel-3A satellite, equipped with Synthetic Aperture Radar (SAR) technology, achieves a ground resolution better than 300 m. This high resolution allows the Sentinel-3A SAR altimeter to effectively avoid land contamination when measuring lake levels, resulting in a larger dataset of valid measurements compared to traditional altimeters. This study utilizes SAR altimeter data from Sentinel-3A, covering 96 cycles, from the second cycle to the most recent 97th cycle, spanning from March 2016 to May 2023. In combination with in situ measurements from tide gauges and GPS buoys, a quantitative observation algorithm for monitoring Qinghai Lake's water levels based on satellite altimetry has been developed.

To obtain accurate and long-term lake surface height data, this study developed a normalization method that derives lake surface heights from Sentinel-3A SAR measurements at various locations relative to a fixed reference point, using geoid height differences. To ensure the precision of geoid height measurements, the first step involves comparing GPS buoy height measurements with in situ tide gauge data. The second step focuses on improving an algorithm for retrieving lake surface height from satellite altimeter data. Finally, filtering and normalization algorithms are applied to generate a time series of lake surface heights based on the Sentinel-3A SAR data.

The precision comparison test of GPS buoy height measurements involved simultaneous measurements with tide gauges and GPS buoys at the same location to assess the accuracy of the GPS buoy height measurements. The test revealed a standard deviation

(StD) of approximately 1.23 cm, indicating that the GPS buoy's height measurement accuracy is around 1 cm, which is sufficient for measuring the geoid height differences at Qinghai Lake. For the satellite-altimeter-based retrieval of lake surface height, this study initially adapted algorithms designed for sea surface height retrieval from satellite altimetry. By analyzing various influencing factors, including tidal correction, sea state bias correction, and load tide correction, a more reasonable lake height inversion algorithm for retrieving lake surface height from satellite altimeter data was established.

In the geoid undulation measurement process, GPS buoys are deployed at the satellite's nadir points via ships, with a tide gauge positioned at the normalization point. A stable one-hour measurement is conducted using the GPS buoy, alongside simultaneous measurements from a pressure-type tide gauge, to determine the geoid height differences between the satellite's nadir points and the normalization point. The experimental results show that the water level fluctuations (standard deviation) measured by the GPS buoy over the one-hour period are all less than 1 cm, demonstrating that the use of GPS buoys to measure geoid height differences is both feasible and accurate. In total, 18 geoid points, including the nadir points of the Sentinel-3A satellite altimeter over Qinghai Lake, have been successfully measured.

This paper presents an inversion algorithm for determining lake surface height from satellite altimeter data, building on existing algorithms for sea surface height inversion. Three data filtering methods—regional filtering, threshold filtering, and altimeter range filtering—were applied to obtain accurate and reliable lake surface height observations from the Sentinel-3A SRAL over Qinghai Lake. Using geoid undulation, the satellite-derived lake surface height data were normalized across different locations and time periods, enabling the construction of a long-term time series. The results show that Qinghai Lake exhibits distinct seasonal variations, with the highest water levels occurring in September and October and the lowest in April and May. Over the seven-year period from 2016 to 2023, the lake's water level rose by 2.41 m, with an average annual increase of 29.9 cm. The rate of increase was 47.2 cm per year from 2016 to 2020, while the water level remained relatively stable from 2020 to 2022.

Observations of inland water bodies are crucial for understanding both local and global climate change. Traditional hydrological station measurements often face limitations in spatial representativeness and temporal continuity. This study leverages Synthetic Aperture Radar (SAR) altimetry data, employing methods such as geoid height difference measurements and normalization algorithms, to generate accurate and reliable long-term time series of lake surface height data for Qinghai Lake. The resulting dataset offers a robust and continuous resource for advancing climate change research.

Taking Qinghai Lake as an example, this article uses satellite altimeter data combined with in situ measurement data to establish an effective satellite data filtering algorithm, make GPS observations of the geoid difference, and obtain accurate and reliable lake water level observation results through the normalization algorithm. The satellite altimeter lake surface height inversion algorithm established in this paper can provide more accurate and real-time data, a basis for the assessment and management of lake water resources, and scientific datasets for the rational use and protection of water resources.

An SAR altimeter is used in this paper, which has a higher along-track spatial resolution than the T/P and Jason altimeter satellites, and although these have more valid data, a higher spatial resolution is needed for lakes to better study lake water levels. As the processing of SWOT satellite altimeter data continues to be optimized, it is expected to provide high-resolution inland water observations with spatial resolutions on the order of 100 m. In the future, the application of satellite altimeter data will enhance our understanding

of lakes, offering deeper insights into their interactions with natural systems and human society, while also clarifying the impacts of these elements on each other.

Author Contributions: C.C. wrote the paper; X.L., C.C., Y.X. and Y.Z. (Yili Zhao) designed and implemented the Sentinel-3A SSH processing scheme; J.Z., H.P. and M.L. designed the Qinghai Lake experiments; W.Z., J.L. and Y.Z. (Yufei Zhang) processed the GPS data. All authors contributed to the discussion and revision of the manuscript. All authors have read and agreed to the published version of the manuscript.

Funding: This research was jointly funded by the Laoshan Laboratory Science and Technology Innovation Projects under Grant LSKJ202201302; the Key Laboratory of Space Ocean Remote Sensing and Application (LORA) Open Fund Project (202101002); the National Natural Science Foundation of China, grant numbers 41406204 and 41501417; and Hainan Province Science and Technology Special Fund (ATIC-202301003).

Data Availability Statement: The GPS buoy, GPSRS, and tide gauge data of the Qinghai Lake experiment were obtained from July to September 2019. The Sentienl-3A SRAL data were obtained from the Copernicus Data Space Ecosystem and are available from https://dataspace.copernicus.eu/explore-data/data-collections/federated-data-sets/, accessed on 21 November 2023.

Acknowledgments: We would like to thank a number of people for contributing to this work, including Youguang Zhang, Zhenzhan Wang, Bonnefond P, Xiyu Xu, Hua Shen, Yanlong Liu, Xiaoxu Zhang, and Qian Zhang for their useful discussions. We would also like to thank the EUMETSAT and Copernicus Data Space Ecosystem for providing free access to the Sentinel-3A Land data, respectively. We also would like to thank MIT and IGS for providing the relevant data.

Conflicts of Interest: The authors declare no conflicts of interest.

References

1. Cretaux, J.F.; Abarca-del-Rio, R.; Berge-Nguyen, M.; Arsen, A.; Drolon, V.; Clos, G.; Maisongrande, P. Lake volume monitoring from space. *Surv. Geophys.* **2016**, *37*, 269–305. [CrossRef]
2. Gao, Q.; Makhoul, E.; Escorihuela, M.J.; Zribi, M.; Seguí, P.Q.; García, P.; Roca, M. Analysis of retrackers' performances and water level retrieval over the Ebro River basin using sentinel-3. *Remote Sens.* **2019**, *11*, 718. [CrossRef]
3. Lee, H.; Shum, C.K.; Tseng, K.H.; Guo, J.Y.; Kuo, C.Y. Present-day lake level variation from envisat altimetry over the northeastern qinghai-tibetan plateau: Links with precipitation and temperature. *Terr. Atmos. Ocean. Sci.* **2011**, *22*, 169–175. [CrossRef]
4. Li, X.Y.; Xu, H.Y.; Sun, Y.L.; Zhang, D.S.; Yang, Z.P. Lake-levelchange and water balance analysis at lake Qinghai, west China during recent decades. *Water Resour. Manag.* **2007**, *21*, 1505–1516. [CrossRef]
5. Lei, Y.B.; Yao, T.D.; Yang, K.; Sheng, Y.W.; Kleinherenbrink, M.; Yi, S.; Bird, B.W.; Zhang, X.W.; Zhu, L.; Zhang, G.Q. Lake seasonality across the Tibetan Plateau and their varying relationship with regional mass changes and local hydrology. *Geophys. Res. Lett.* **2017**, *44*, 892–900. [CrossRef]
6. Tang, M.; Gao, X.; Zhang, J. Interannual changes in the water level of Qinghai Lake over the past 30 years. *Sci. Bull.* **1992**, *37*, 524–527.
7. Haines, B.; Desai, S.; Shah, R.; Leben, B.; Masters, D.; Meinig, S.C.; Nerem, S.S. The Harvest Experiment: Connecting Jason-3 to the Long-Term Sea Level Record. In Proceedings of the 2016 OSTST Meeting, La Rochelle, France, 1–4 November 2016.
8. Bonnefond, P.; Laurain, O.; Exertier, P.; Boy, F.; Guinle, T.; Picot, N.; Labroue, S.; Raynal, M.; Donlon, C.; Féménias, P.; et al. Calibrating the SAR SSH of Sentinel-3A and CryoSat-2 over the Corsica Facilities. *Remote Sens.* **2018**, *10*, 92. [CrossRef]
9. Mertikas, S.P.; Donlon, C.; Féménias, P.; Mavrocordatos, C.; Galanakis, D.; Tripolitsiotis, A.; Frantzis, X.; Tziavos, I.N.; Vergos, G.; Guinle, T. Fifteen Years of Cal/Val Service to Reference Altimetry Missions: Calibration of Satellite Altimetry at the Permanent Facilities in Gavdos and Crete, Greece. *Remote Sens.* **2018**, *10*, 1557. [CrossRef]
10. Chen, C.T.; Zhu, J.H.; Zhai, W.L.; Yan, L.H.; Zhao, Y.L.; Huang, X.Q.; Yang, W.W. Absolute calibration of HY-2A and Jason-2 Altimeters for sea surface height using GPS buoy in Qinglan, China. *J. Oceanol. Limnol.* **2019**, *37*, 1533–1541. [CrossRef]
11. Birkett, C.M. The contribution of TOPEX/POSEIDON to the global monitoring of climatically sensitive lakes. *J. Geophys. Res.* **1995**, *100*, 25179–25204. [CrossRef]
12. Gao, L.; Liao, J.J.; Shen, G.Z. Monitoring lake-level change in the Qinghai-Tibetan Plateau using radar altimeter data (2002–2012). *Appl. Remote Sens.* **2013**, *7*, 073470-1–073470-17. [CrossRef]

13. Kleinherenbrink, M.; Ditmar, P.G.; Lindenbergh, R.C. Retracking Cryosat data in the SARIn mode and robust lake level extraction. *Remote Sens. Environ.* **2014**, *152*, 38–50. [CrossRef]
14. Kleinherenbrink, M.; Lindenbergh, R.C.; Ditmar, P.G. Monitoring of lake level changes on the Tibetan Plateau and Tian Shan by retracking Cryosat SARIn waveforms. *J. Hydrol.* **2015**, *521*, 119–131. [CrossRef]
15. Medina, C.E.; Gomez-Enri, J.; Alonso, J.J.; Villares, P. Water level fluctuations derived from ENVISAT Radar Altimeter (RA-2) and in-situ measurements in a subtropical waterbody: Lake Izabal (Guatemala). *Remote Sens. Environ.* **2008**, *112*, 3604–3617. [CrossRef]
16. Song, C.; Ye, Q.; Sheng, Y.; Gong, T. Combined ICESat and CryoSat-2 Altimetry for Accessing Water Level Dynamics of Tibetan Lakes over 2003–2014. *Water* **2015**, *7*, 4685–4700. [CrossRef]
17. Wang, X.W.; Gong, P.; Zhao, Y.; Xu, Y.; Cheng, X.; Niu, Z.; Luo, Z.; Huang, H.; Sun, F.; Li, X. Water-level changes in China's large lakes determined from ICESat/GLAS data. *Remote Sens. Environ.* **2013**, *132*, 131–144. [CrossRef]
18. Gao, Y. Lake Level Variations from Satellite Altimetry. Master's Thesis, Hohai University, Nanjing, China, 2006.
19. Wen, J. Research and Application on the Satellite Altimetery Data to Monitor the Water Level of Lakes and Reservoirs in China. Master's Thesis, Lanzhou Jiaotong University, Lanzhou, China, 2018.
20. Tong, X.; Pan, H.; Xie, H.; Xu, X.; Li, F.; Chen, L.; Luo, X.; Liu, S.; Chen, P.; Jin, Y. Estimating water volume variations in Lake Victoria over the past 22 years using multi-mission altimetry and remotely sensed images. *Remote Sens. Environ.* **2016**, *187*, 400–413. [CrossRef]
21. Zhang, G.; Yao, T.; Shum, C.K.; Yi, S.; Yang, K.; Xie, H.; Feng, W.; Bolch, T.; Wang, L.; Behrangi, A.; et al. Lake volume and groundwater storage variations in Tibetan Plateau's endorheic basin. *Geophys. Res. Lett.* **2017**, *44*, 5550–5560. [CrossRef]
22. Cai, Y. Multi-Source Remote Sensing Data Application Study on Poyang Lake Water Environment. Ph.D. Thesis, Institute of Remote Sensing Applications, Chinese Academy of Sciences, Beijing, China, 2006.
23. Wu, H.; Chen, Y. Estimation of lake water storage change of Qinghai Lake based on the ICESat satellite altimetry data and Landsat satellite imageries. *J. Water Resour. Water Eng.* **2022**, *31*, 7–15.
24. Zhang, G.; Xie, H.; Ysao, T.; Kang, S. Water balance estimates of ten greatest lakes in Chian using ICESat and Landsat data. *Sci. Bull.* **2013**, *26*, 2664–2678.
25. Berry, P.A.M.; Garlick, J.D.; Freeman, J.A.; Mathers, E.L. Global inland water monitoring from multi-mission altimetry. *Geophys. Res. Lett.* **2005**, *32*, L16401. [CrossRef]
26. Frappart, F.; Calmant, S.; Cauhope, M.; Seyler, F.; Cazenave, A. Preliminary results of ENVISAT RA-2-derived water levels validation over the Amazon basin. *Remote Sens. Environ.* **2006**, *100*, 252–264. [CrossRef]
27. Alsdorf, D.; Birkett, C.M.; Dunne, T.; Melack, J.; Hess, L. Water level changes in a large Amazon lake measured with spaceborne radar interferometry and altimetry. *Geophys. Res. Lett.* **2001**, *28*, 2671–2674. [CrossRef]
28. Boergens, E.; Dettmering, D.; Schwatke, C.; Seitz, F. Treating the hooking effect in satellite altimetry data: A case study along the Mekong River and its tributaries. *Remote Sens.* **2016**, *8*, 91. [CrossRef]
29. Villadsen, H.; Andersen, O.B.; Stenseng, L.; Nielsen, K.; Knudsen, P. CryoSat-2 altimetry for river level monitoring—Evaluation in the Ganges-Brahmaputra River basin. *Remote Sens. Environ.* **2015**, *168*, 80–89. [CrossRef]
30. Birkett, C.M. Contribution of the TOPEX NASA Radar Altimeter to the global monitoring of large rivers and wetlands. *Water Resour. Res.* **1998**, *34*, 1223–1239. [CrossRef]
31. Santos da Silva, J.; Calmant, S.; Seyler, F.; Filho, O.C.R.; Cochonneau, G.; Mansur, W.J. Water levels in the Amazon basin derived from the ERS 2 and ENVISAT radar altimetry missions. *Remote Sens. Environ.* **2010**, *114*, 2160–2181. [CrossRef]
32. Kim, J.-W.; Lu, Z.; Lee, H.; Shum, C.; Swarzenski, C.M.; Doyle, T.W.; Baek, S.-H. Integrated analysis of PALSAR/Radarsat-1 In SAR and ENVISAT altimeter data for mapping of absolute water level changes in Louisiana wetlands. *Remote Sens. Environ.* **2009**, *113*, 2356–2365. [CrossRef]
33. Lee, H.; Yuan, T.; Jung, H.C.; Beighley, E. Mapping wetland water depths over the central Congo Basin using PALSAR Scan SAR, Envisat altimetry, and MODIS VCF data. *Remote Sens. Environ.* **2015**, *159*, 70–79. [CrossRef]
34. Wang, N. Research and Implementation of River Runoff Monitoring System Based on Multi-Source Radar Remote Sensing Technology. Master's Thesis, Henan University, Kaifeng, China, 2019.
35. Yuan, C. Applied Research on Radar Altimetry over Inland Waters. Ph.D. Thesis, Institute of Remote Sensing and Digital Earth, Graduate University of Chinese Academy of Sciences, Beijing, China, 2017.
36. Zhao, Y. Method of Monitoring Water Level Change of Main Lakes in China with Radar Altimeter Data. Ph.D. Thesis, Institute of Remote Sensing and Digital Earth, Graduate University of Chinese Academy of Sciences, Beijing, China, 2017.
37. Fu, L.L.; Cazenave, A. *Satellite Altimetry and Earth Sciences: A Handbook of Techniques and Applications*; Academic Press: San Diego, CA, USA, 2001; pp. 407–435.
38. Cretaux, J.-F.; Calmant, S.; Romanovsky, V.; Perosanz, F.; Tashbaeva, S.; Bonnefond, P.; Moreira, D.; Shum, C.K.; Nino, F.; Bergé-Nguyen, M.; et al. Absolute Calibration of Jason radar altimeters from GPS kinematic campaigns over Lake Issykkul. *Mar. Geod.* **2011**, *34*, 291–318. [CrossRef]

39. Cretaux, J.F.; Berge-Nguyen, M.; Calmant, S.; Jamangulova, N.; Satylkanov, R.; Lyard, F.; Perosanz, F.; Verron, J.; Montazem, A.S.; Guilcher, G.L.; et al. Absolute Calibration or Validation of the Altimeters on the Sentinel-3A and the Jason-3 over Lake Issykkul (Kyrgyzstan). *Remote Sens.* **2018**, *10*, 92. [CrossRef]
40. Chen, J.; Liao, J. Monitoring lake level changes in China using multi-altimeter data (2016–2019). *J. Hydrol.* **2020**, *590*, 125544. [CrossRef]
41. Available online: https://sentiwiki.copernicus.eu/web/s3-altimetry-instruments (accessed on 22 June 2024).
42. Copernicus S3: Product Notic eAltimetry: S3.PN-STM-L1L-L2L—Issue 1.4—17/06/2024. Contract: 4000136824/21/I-BG. Available online: https://sentiwiki.copernicus.eu/__attachments/1672112/S3A.PN-STM-L1L-L2L%20-%20Sentinel%203%20Product%20Notice%20Altimetry%20(PB3.29)%202024%20-%201.4.pdf?inst-v=c9602fd8-862c-4637-a9c5-f5e318bba7ca (accessed on 22 June 2024).
43. Cao, Y.; Lin, C.; Zhang, X. Distribution and Geochemical Processes of Arsenic in Lake Qinghai Basin, China. *Water* **2021**, *13*, 1091. [CrossRef]
44. Zhao, Y.; Liao, J.J.; Shen, G.Z.; Zhang, X.L. Monitoring the water level changes in Qinghai Lake with satellite altimetry data. *J. Remote Sens.* **2017**, *21*, 633–644. [CrossRef]
45. Chen, C.T.; Zhai, W.L.; Yan, L.H.; Zhang, Q.; Zhang, X.X.; Zhu, J.H.; He, S.Y. Assessment of the GPS Buoy Accuracy for Altimeter Sea Surface Height Calibration. In Proceedings of the 2014 IEEE Geoscience and Remote Sensing Symposium (IGARSS), Quebec City, QC, Canada, 13–18 July 2014; pp. 3101–3104.
46. Zhai, W.; Zhu, J.; Chen, C.; Yan, L.; Tian, Z. Calibration and Validation of Satellite Altimeters in Qinghai Lake. In Proceedings of the 2022 IEEE International Geoscience and Remote Sensing Symposium (IGARSS), Kuala Lumpur, Malaysia, 17–22 July 2022; pp. 7010–7013. [CrossRef]
47. Herring, T.A.; King, R.W.; McClusky, S.C. GAMIT Reference Manual: GPS at MIT (Release.10.4) [M/OL]. Massachusetts Institute of Technology. 28 October 2010. Available online: https://www.scirp.org/reference/referencespapers?referenceid=1556938 (accessed on 22 June 2020).
48. Herring, T.; King, R.; McClusky, S. *Introduction to GAMIT/GLOBK (Release 10.7)*; Massachusetts Institute of Technology: Cambridge, MA, USA. Available online: http://geoweb.mit.edu/gg/Intro_GG.pdf (accessed on 22 June 2020).
49. Herring, T.A. *TRACK GPS Kinematic Positioning Program, Version 1.07*; Massachusetts Institute of Technology: Cambridge, MA, USA, 2012.
50. Wang, G. Lake Ice Characteristics and Changes in Qinghai Lake. Master's Thesis, Lanzhou University, Lanzhou, China, 2020.
51. Jiang, W.P.; Chu, Y.H.; Li, J.C.; Yao, Y.S. Water level variation of Qinghai Lake from altimeteric data. *Geomat. Inf. Sci. Wuhan Univ.* **2008**, *33*, 64–67.
52. Li, T.; Li, N.; Wang, Y. Dynamic monitoring of the water area of Qinghai Lake. *J. Qinghai Univ.* **2016**, *34*, 49–54.
53. Lei, Y.; Yang, K.; Wang, B.; Sheng, Y.; Bird, B.W.; Zhang, G.; Tian, L. Response of inland lake dynamics over the Tibetan Plateau to climate change. *Clim. Chang.* **2014**, *125*, 281–290. [CrossRef]
54. Song, C.; Huang, B.; Richards, K.; Ke, L.; Hien, V.P. Accelerated lake expansion on the Tibetan Plateau in the 2000s: Induced by glacial melting or other processes? *Water Resour. Res.* **2014**, *50*, 3170–3186. [CrossRef]
55. Biskop, S.; Maussion, F.; Krause, P.; Fink, M. Differences in the water-balance components of four lakes in the southern-central Tibetan Plateau. *Hydrol. Earth Syst. Sci.* **2016**, *20*, 209–225. [CrossRef]
56. Li, B.; Zhang, J.; Yu, Z.; Liang, Z.; Chen, L.; Acharya, K. Climate change driven water budget dynamics of a Tibetan inland lake. *Glob. Planet Chang.* **2017**, *150*, 70–80. [CrossRef]
57. Zhou, J.; Wang, L.; Zhang, Y.; Guo, Y.; Li, X.; Liu, W. Exploring the water storage changes in the largest lake (Selin Co) over the Tibetan Plateau during 2003–2012 from a basin-wide hydrological modeling. *Water Resour. Res.* **2015**, *51*, 8060–8086. [CrossRef]
58. Brun, F.; Treichler, D.; Shean, D.; Immerzeel, W.W. Limited Contribution of Glacier Mass Loss to the Recent Increase in Tibetan Plateau Lake Volume. *Front. Earth Sci.* **2020**, *8*, 582060. [CrossRef]
59. Zhang, G.; Bolch, T.; Chen, W.; Crétaux, J.F. Comprehensive estimation of lake volume changes on the Tibetan Plateau during 1976–2019 and basin-wide glacier contribution. *Sci. Total Environ.* **2021**, *772*, 145463. [CrossRef] [PubMed]
60. Liu, J.; Liu, J.; Li, X.; Wang, J.; Ma, S. Application of domestic marine satellite data in inland areas—A case study of Qinghai. *Manag. Strategy Qinghai Land Resour.* **2021**, *5*, 56–58.

Disclaimer/Publisher's Note: The statements, opinions and data contained in all publications are solely those of the individual author(s) and contributor(s) and not of MDPI and/or the editor(s). MDPI and/or the editor(s) disclaim responsibility for any injury to people or property resulting from any ideas, methods, instructions or products referred to in the content.